J. Fluid Mech. (1975), *vol.* 69, *part* 2, *pp.* 263–282
Printed in Great Britain

The effect of turbulence on the surface pressure field of a square prism

By B. E. LEE
Department of Building Science, Sheffield University

(Received 29 May 1974)

Measurements are presented of the mean and fluctuating pressure field acting on a two-dimensional square cylinder in uniform and turbulent flows. The addition of turbulence to the flow is shown to raise the base pressure and reduce the drag of the body. It is suggested that this is attributable to the manner in which the increased turbulence intensity thickens the shear layers, which causes them to be deflected by the downstream corners of the body and results in the downstream movement of the vortex formation region. The strength of the vortex shedding is shown to be reduced as the intensity of the incident turbulence is increased.

1. Introduction

It is required that buildings and structures shall not suffer damage due to wind loading and that they shall be designed economically. Since it would be unrealistic to perform fluctuating wind loading tests on a complete building at the present time, owing to the considerable amount of experimentation this would necessitate, it is desirable that a theoretical or empirical solution be applied to simplify the problem. But development of such an approach is hampered by our lack of understanding of some of the important flow phenomena.

Another problem of practical importance is that, according to a strict interpretation of the scaling laws, it is necessary to simulate the intensity and scale of the atmospheric turbulent flow incident on building models in the wind tunnel. But the scales and intensities of atmospheric turbulence are not known with absolute precision. It is necessary to know how sensitive the wind loads are to changes in the incident turbulence structure. If the loads are insensitive, existing atmospheric turbulence data will be adequate; conversely, if the loads are sensitive, more precise full-scale data will be required. Hence, the results of this work are intended to give an indication of the accuracy that ought to be achieved in wind tunnel simulations of atmospheric flows.

While the fluctuating forces and the associated vortex shedding from a circular cylinder have been the subject of considerable research, comparatively little attention has been paid to other bluff body shapes. Little information is available on the effects of turbulence on vortex shedding from sharp edged bluff structures, although this is a problem of considerable practical significance. As part of a research programme aimed at improving our knowledge in this field,

the aerodynamics of a two-dimensional square-section prismatic cylinder immersed in a grid-produced turbulent fluid stream have been studied. In the part of the study reported here, only the surface pressure field is under consideration. The simplification of two-dimensionality and flow homogeneity allows some of the conflicting effects occurring in a real flow situation to be studied in isolation, enabling one to gain an insight into their individual importance.

2. Experimental equipment

2.1. *Details of model*

The model used in this study was a square prismatic cylinder, measuring 165×165 mm, which spanned the working section of the CERL $4{\cdot}58 \times 1{\cdot}53$ m Low Speed Wind Tunnel. The model was mounted at the centre of the turntable across the shorter dimension of the tunnel. It was manufactured from 6·4 mm thick aluminium plates bolted together at the corners and machined to give a smooth surface with sharp edges. The model was strengthened internally with web plates. The model orientation was such that, at an angle of incidence α of 0°, face (*a*) was the windward face normal to the flow, faces (*b*) and (*d*) were parallel to the flow and face (*c*) was the leeward face. At $\alpha = 90°$, face (*b*) became the windward normal face and face (*d*) the leeward face. At $\alpha = 0$ the blockage ratio was 3·6 % and the length/D ratio was 9·2 (D is the prism side length).

Pressure tappings were provided as follows. (i) A part circumferential ring of 18 tappings was located at the mid-span, consisting of 6 equidistant tappings on the three faces (*a*)–(*c*). Tappings were omitted on face (*d*) of the model, since it was necessary to remove this face, to gain access to the inside of the prism. The results for face (*d*) were obtained by symmetry. The tapping numbering system is indicated on the axes of figures 1 and 2. (ii) Three axial rows of 12 tappings were each provided on face (*a*), which spanned the accessible length of the model. The length of this span was limited to 0·7 m by the internal web plates. These three axial rows of tappings were in line with tappings 1, 2 and 3 on the circumferential ring. All the tappings were 9·5 mm deep, and had a 0·56 mm bore.

2.2. *Details of turbulence-producing grids*

Various intensities and scales of incident flow turbulence were produced by square mesh grids upstream of the model. These grids consisted of flat aluminium bars, 3·2 mm thick and of various widths, bolted to T-section aluminium struts of the same thickness and frontal width in the form of a bi-plane square mesh grid. Details of the bar width, mesh size and distance upstream of the model are given in table 1, together with their turbulence properties. L_1 and L_2 denote the lateral and longitudinal integral length scales of the u component of turbulence, respectively.

2.3. *Details of instruments*

Measurements of the fluctuating pressures were made using S.E. Laboratories differential pressure transducers. The connecting pipe lengths between the transducers and the pressure tappings varied from 25·4 to 153 mm. An analog

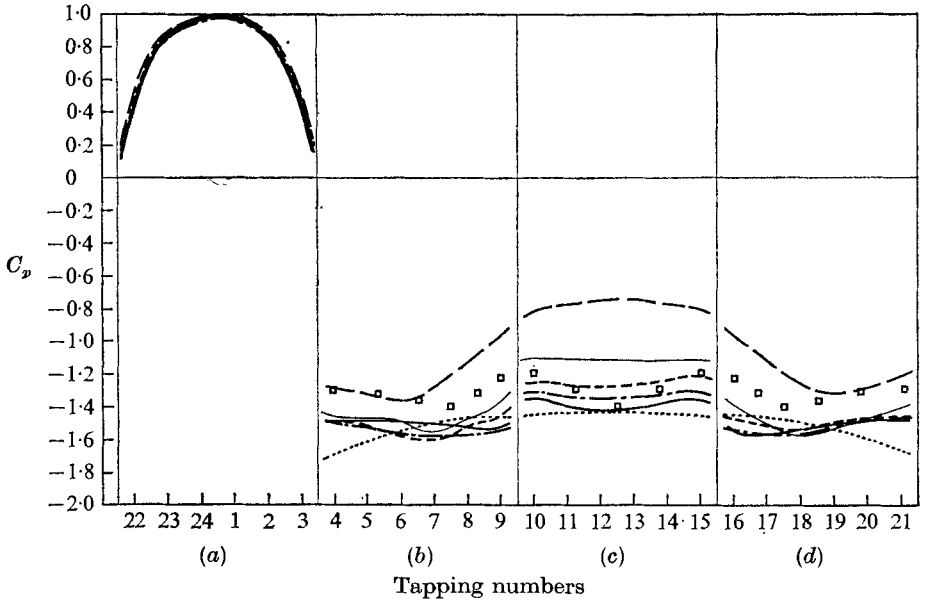

FIGURE 1. Mean pressure distribution at $\alpha = 0°$. Uniform flow: ——, smooth flow: ·····, Engineering Sciences Data Unit (1971), data sheet 71016; □, Pocha (1971).

Grid	A1	A2	A3	A4

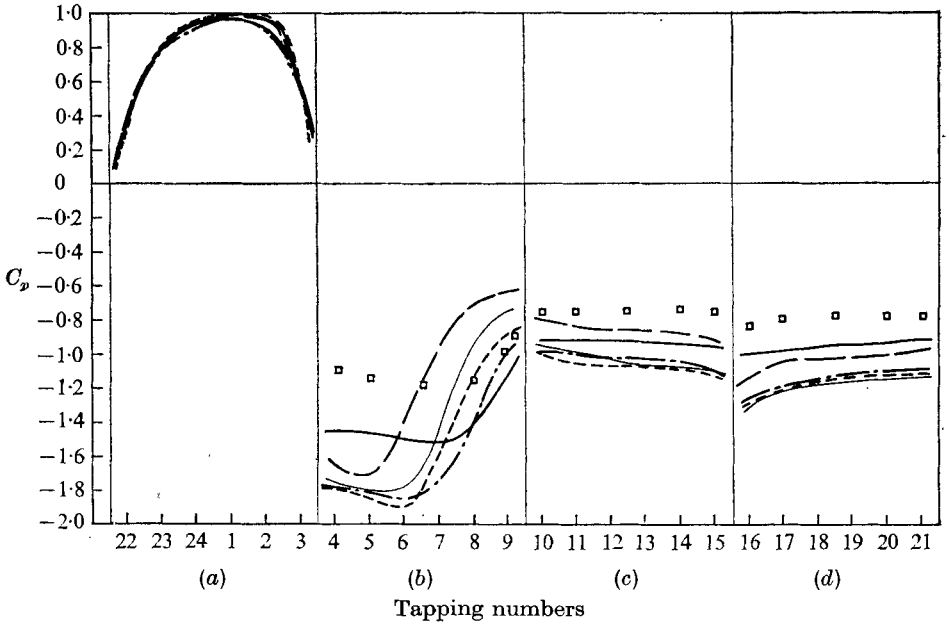

FIGURE 2. Mean pressure distribution at $\alpha = 12° 30'$. Faces (*a*)–(*d*).
(For symbol key, see caption to figure 1.)

Grid number	$\frac{(\overline{u^2})^{\frac{1}{2}}}{U}$ %	L_1 (m)	L_2 (m)	$\frac{L_2}{D}$	Upstream distance (m)	Bar size (mm)	Mesh size (m)
Uniform flow	0·5						
A1	4·4	0·063	0·160	0·97	6·9	50·8	0·31
A2	6·5	0·072	0·188	1·14	6·9	88·9	0·51
A3	8·0	0·049	0·120	0·73	3·65	50·8	0·31
A4	12·5	0·046	0·155	0·94	3·65	88·9	0·51

TABLE 1. Properties of grid-generated turbulence

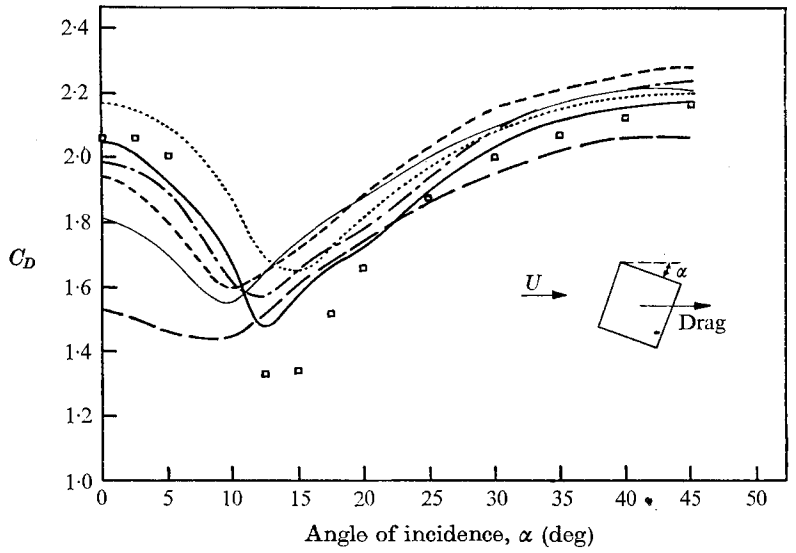

FIGURE 3. Variation of mean drag coefficient with flow direction. (For symbol key, see caption to figure 1.)

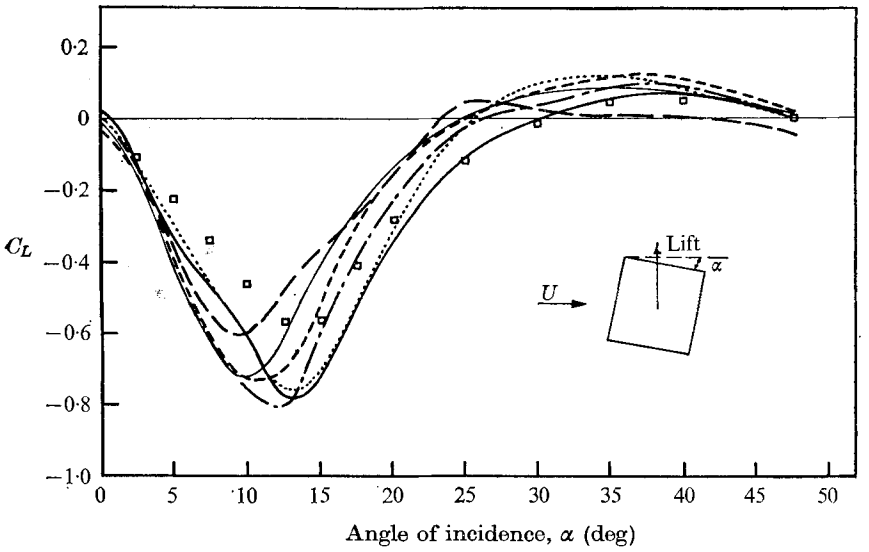

FIGURE 4. Variation of mean lift coefficient with flow direction. (For symbol key, see caption to figure 1.)

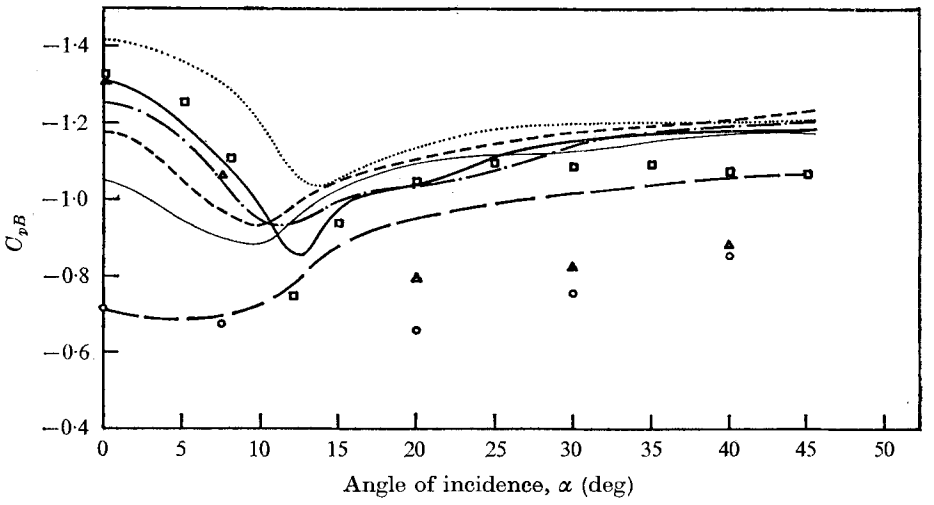

FIGURE 5. Variation of base pressure with flow direction. △, Vickery (1966), smooth flow; ○, 10% turbulent flow. (For key to other symbols, see caption to figure 1.)

filter was placed between the pressure transducer output and the data processing or recording equipment, to give the frequency response a sharp cut-off at 130 Hz. The pressure transducer outputs were processed on-line by the multi-channel Correlator Unit, developed at CERL, to give the variances and correlations of 12 data channels simultaneously.

Analog data recordings were also made on a Sangamo 3500 series tape recorder and analysed on a Honeywell 9300 analyser, to give power spectral densities of the pressure fluctuations. A sample length of data of 600 s was required to give sufficient resolution at low frequencies.

3. Experimental results

Tests were conducted on the square prism in a uniform flow and in homogeneous turbulent flows at $Re = 1{\cdot}76 \times 10^5$.

The mean pressure distributions C_p for angles of incidence of the prism of $\alpha = 0°$ and 12° 30′ are shown in figures 1 and 2, respectively. The mean drag and lift coefficients C_D and C_L, respectively, were determined by integrating the mean pressure distributions and are shown in figures 3 and 4 for $0 \leqslant \alpha \leqslant 45°$. The mean lift and drag coefficients are non-dimensionalized with respect to D as the reference length (not the length projected normal to the flow). The variation of the base pressure C_{pB}, with α increasing from 0 to 45°, is shown in figure 5. The base pressure is defined as the average of the pressures on the mid and quarter points of the leeward face (face (*c*)).

The mean drag, mean lift and base pressure coefficients have been corrected for wind tunnel blockage by the method of Allen & Vincenti (1944). The maximum correction to the mean free-stream velocity was 3%, the corresponding corrections to the mean drag, mean lift and base pressure coefficients being 7, 4 and 10%, respectively. The use of this type of blockage correction assumes

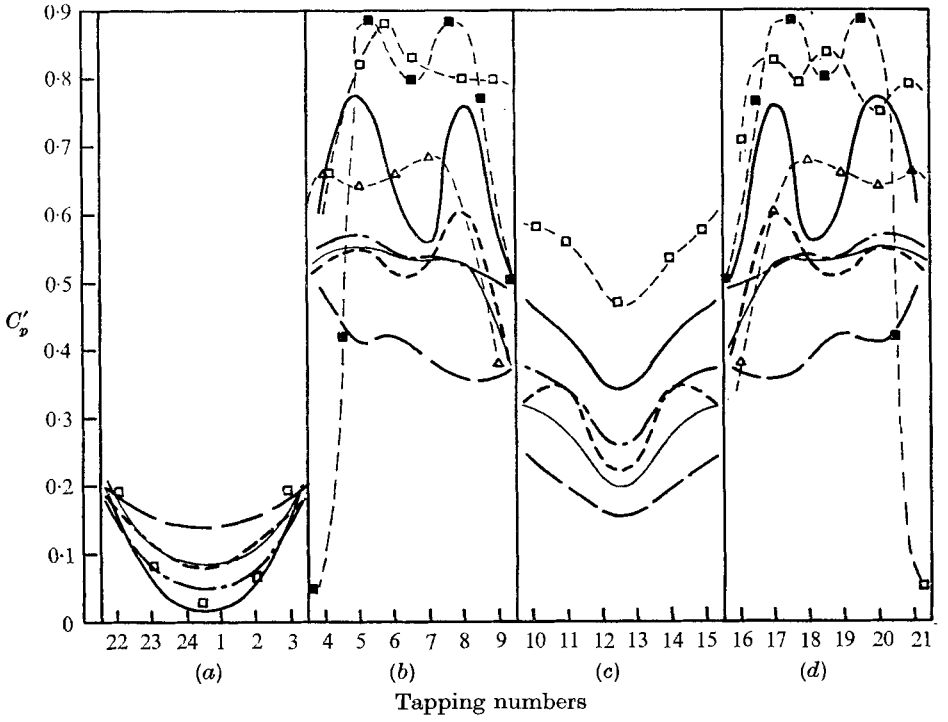

FIGURE 6. Distribution of C'_p at $\alpha = 0°$. Faces (*a*)–(*d*). Smooth flow: △, Chaplin & Shaw (1971); ■, Vickery (1966). (For key to other symbols, see caption to figure 1.)

that the pressure distribution is independent of Reynolds number. The r.m.s. fluctuating pressure distribution C'_p, for an angle of incidence of the prism of $\alpha = 0°$, is shown in figure 6. No blockage corrections have been applied to these data.

Axial correlation coefficients $R(p,z)$ of the surface pressure fluctuations were obtained for each of the three rows of axial pressure tapping positions at angles of $\alpha = 0$, 15, 30 and 45°. The more significant results are presented in figures 7–9. The associated axial correlation length scales were calculated for $\alpha = 0°$. Some of these are presented in table 2 for measurements on the first row of tappings (i.e. those at a distance $\frac{1}{2}D$ from the centre-line of the face). A complete circumferential correlation matrix was obtained for each of the five incident flow conditions for angles of incidence of $\alpha = 0$, 15, 30 and 45°; the more significant results are shown in figures 10 and 11. From these correlation coefficients the covariance matrices were formed; hence, the fluctuating force coefficients C'_X and C'_Y were deduced. They are presented in figures 12 and 13 as a function of the angle of incidence α. From the covariance matrices, the eigenvalues and eigenvector distributions were also extracted. The eigenvector distribution for the leading eigenvalue at $\alpha = 0$ is shown in figure 14. The relative magnitudes of the sum of the eigenvalues and the contributions of the leading five eigenvalues to that sum for all flow conditions at angles of incidence of $\alpha = 0$, 15, 30 and 45° are shown in table 3.

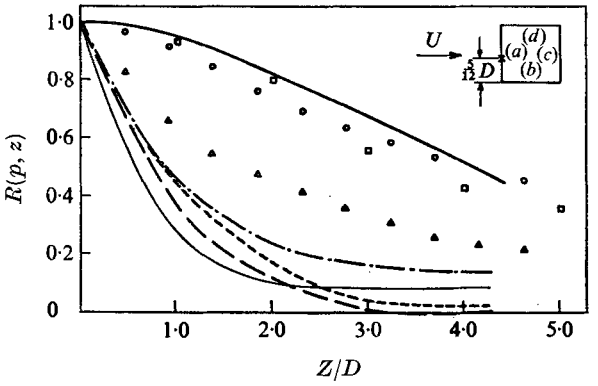

FIGURE 7. Axial correlation coefficient $R(p, z)$ on face (a) at $\alpha = 0°$. Vickery (1966), centre-line measurements: ○, smooth flow; △, turbulent. (For key to other symbols, see caption to figure 1.)

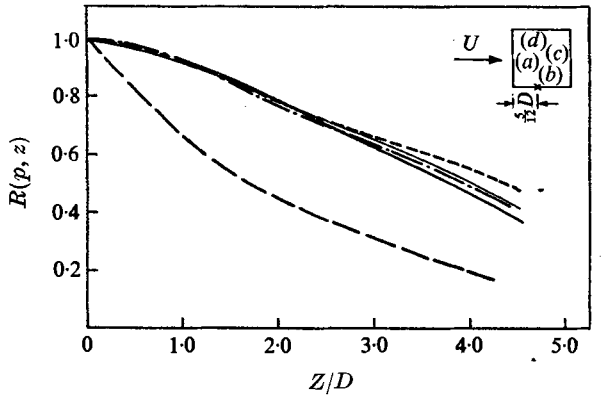

FIGURE 8. Axial correlation coefficient $R(p, z)$ on face (b) at $\alpha = 0°$. (For symbol key, see caption to figure 1.)

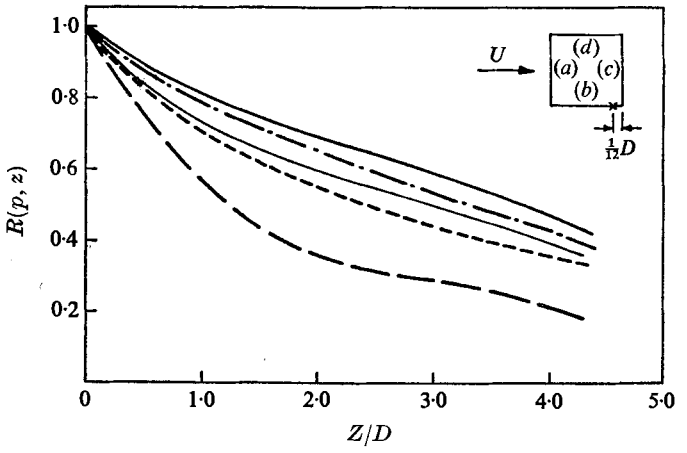

FIGURE 9. Axial correlation coefficient $R(p, z)$ on face (c) at $\alpha = 0°$. (For symbol key, see caption to figure 1.)

Flow	Prism face	Axial correlation length scale
Uniform flow	(*a*)	4·1*D*
Grid A4: 12·5% turbulence intensity	(*a*)	0·96*D*
Uniform flow	(*c*)	1·2*D*
Grid A4: 12·5% turbulence intensity	(*c*)	1·4*D*

TABLE 2. Axial length scales at $\alpha = 0$

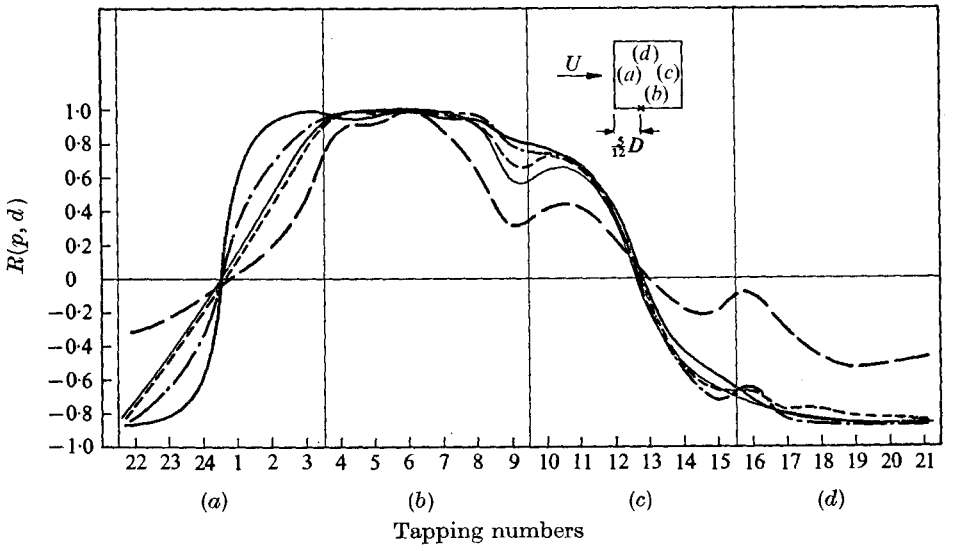

FIGURE 10. Circumferential correlation coefficient $R(p, d)$ distribution with respect to tapping 6 at $\alpha = 0°$. (For symbol key, see caption to figure 1.)

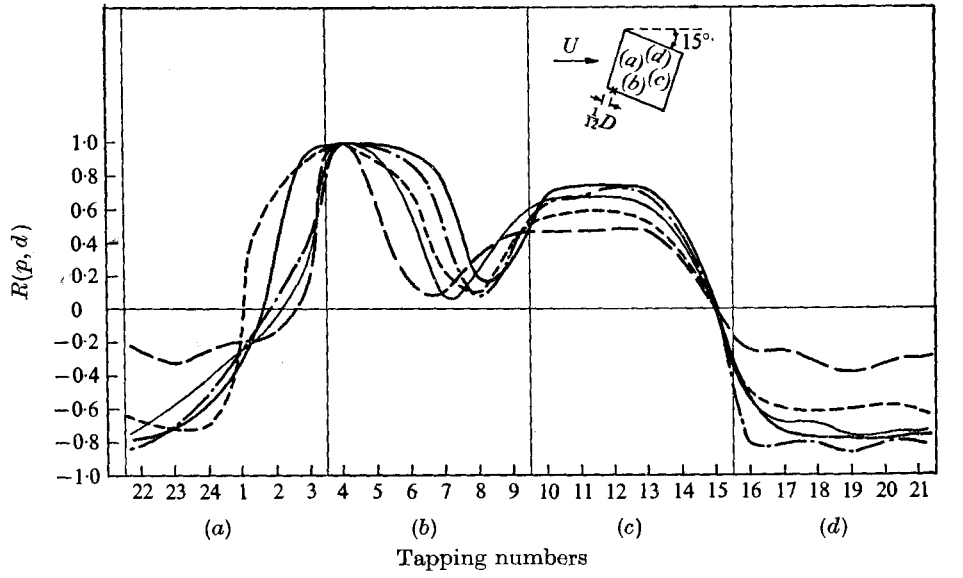

FIGURE 11. Circumferential correlation coefficient $R(p, d)$ distribution with respect to tapping 4 at $\alpha = 15°$. (For symbol key, see caption to figure 1.)

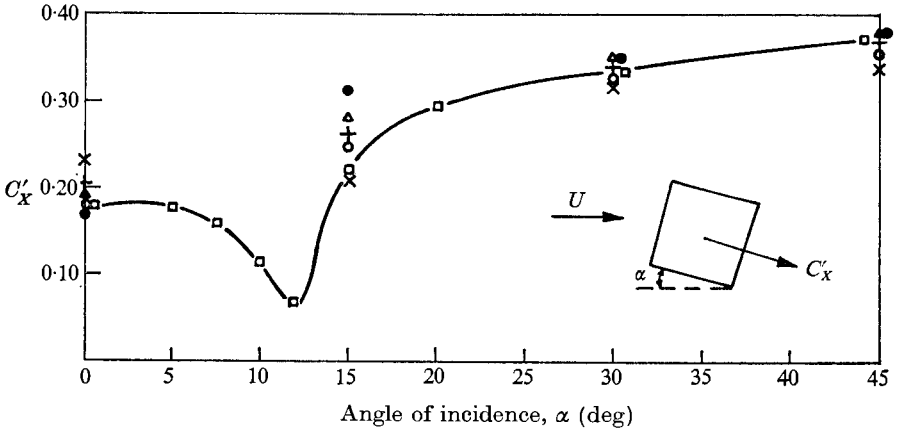

FIGURE 12. Variation of C'_X with flow direction. ×, uniform flow; □, Pocha (1971), smooth flow.

Grid	A1	A2	A3	A4
	○	+	●	△

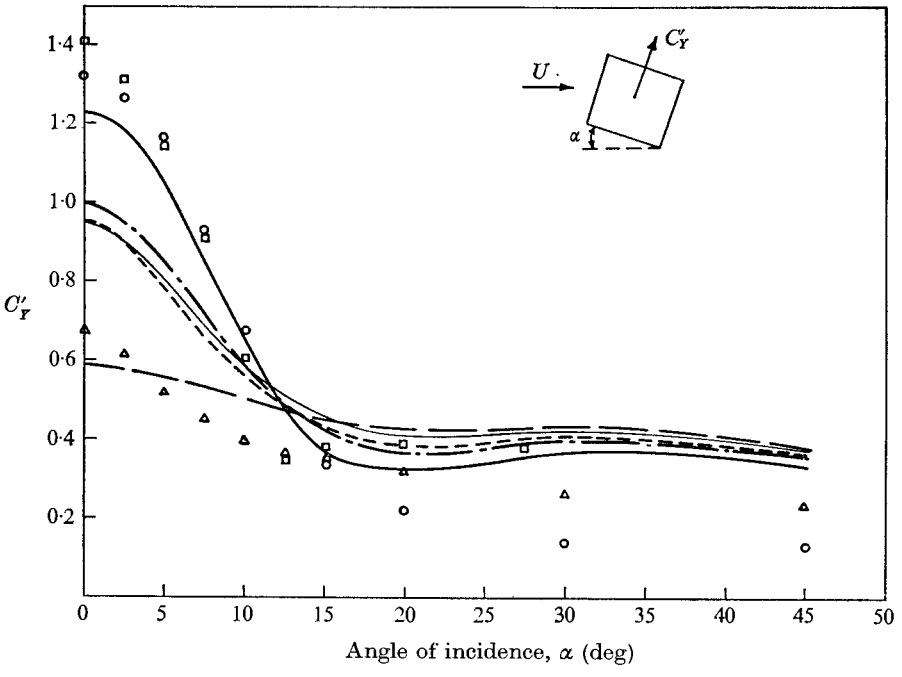

FIGURE 13. Variation of C'_Y with flow direction. Vickery (1966): ○, smooth flow; △, turbulent. (For key to other symbols, see caption to figure 1.)

Power spectral densities of the pressure fluctuations measured at various positions on the prism for an angle of incidence $\alpha = 0°$ are presented in figures 15 and 16. No effect of incident turbulence scale was found in the range investigated.

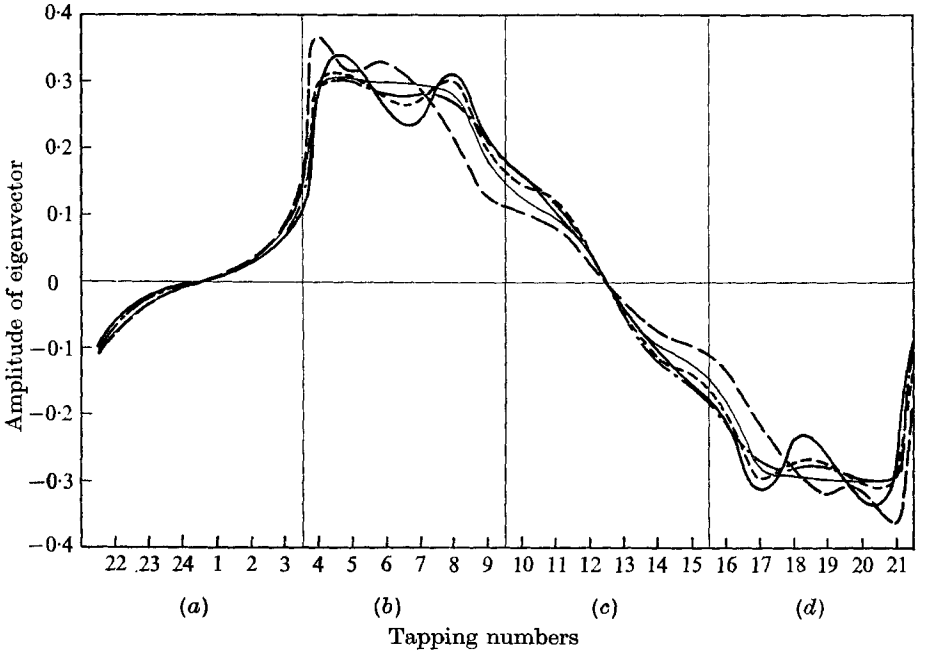

FIGURE 14. First eigenvector distribution, $\alpha = 0°$. Faces (*a*)–(*d*).
(For symbol key, see caption to figure 1.)

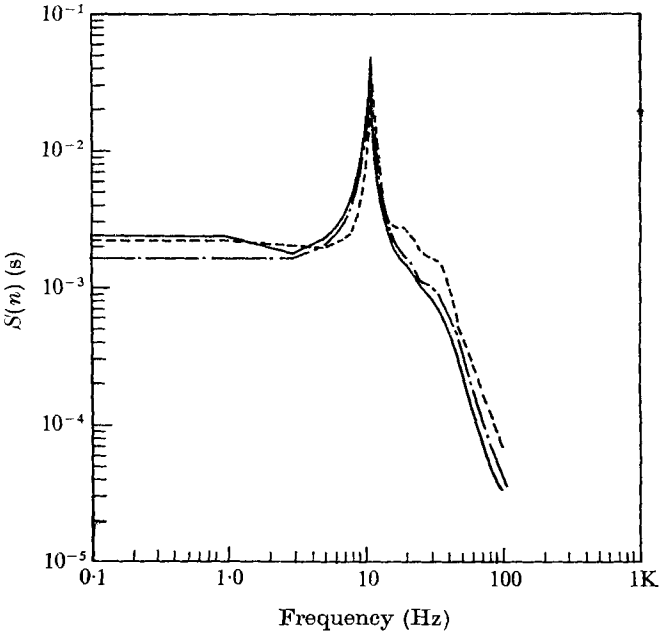

FIGURE 15. Spectra of surface pressures on side face. Grid A4 at $\alpha = 0°$.

	Tapping	C'_p
———	7	0·384
—— · ——	8	0·354
— — — —	9	0·363

Flow condition	α	Sum of eigen-values	% 1st eigen-value	% 2nd eigen-value	% 3rd eigen-value	% 4th eigen-value	% 5th eigen-value	% total contribution of first 5 eigenvalues
Uniform flow	0	6·31	79·7	7·3	3·8	2·3	1·7	94·8
	15	0·98	59·0	16·9	6·9	4·3	3·3	90.4
	30	1·50	50·2	26·1	9·6	5 2	3·2	94·3
	45	1.54	47·2	29·5	10·5	5·6	3·0	95·8
Grid A1	0	4·21	80·2	5·7	5·6	2·4	1·4	95·3
	15	1·32	61·4	15·0	6·9	5·2	3·9	92·4
	30	1·55	58·0	23·3	8·0	4·0	1·7	95·1
	45	1·52	59·1	22·7	7·2	5·4	1·5	95·9
Grid A2	0	4·00	76·0	8·3	5·1	2·9	2·6	94·9
	15	1·60	49·7	19·6	9·6	5·4	5·0	89·3
	30	1·67	56·6	23·0	7·8	3·7	2·0	93·1
	45	1·69	52·4	28·9	6·8	3·4	2·9	94·4
Grid A3	0	3·81	77·9	5·1	3·5	3·3	3·1	92·9
	15	1·89	53·3	17·4	8·5	5·5	5·1	89·9
	30	1·84	54·1	21·7	10·8	6·4	2·4	95·4
	45	1·80	55·3	23·4	9·2	5·1	2·0	95·0
Grid A4	0	2·33	49·2	18·1	6·7	6·4	4·4	84·8
	15	1·97	43·9	17·8	11·0	6·5	4·5	83·7
	30	2·04	50·2	22·7	7·6	7·2	4·0	91·7
	45	1·88	50·7	27·6	5·9	4·9	3·3	92·4

TABLE 3. Eigenvalue table

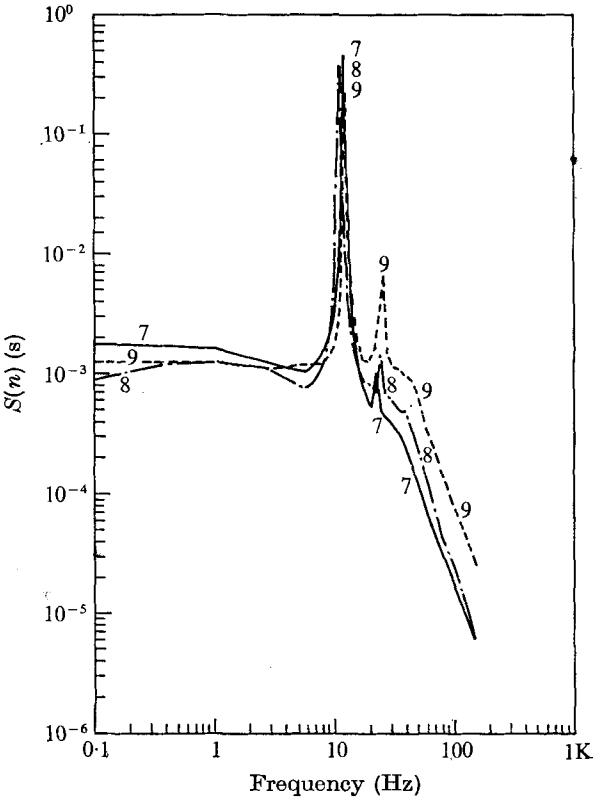

FIGURE 16. Spectra of surface pressures on side face. Grid A3 at $\alpha = 0°$.

	Tapping	C'_p
———	7	0·536
—·—	8	0·530
– – –	9	0·436

4. Discussion

In considering the pressure field acting on a sharp-edged bluff body, there are two major parameters that affect the flow. The first of these is the type of incident flow, be it uniform, sheared or turbulent, with varying length scales and intensities. The second of these parameters is the attitude of the sides of the body to the flow. Though the influence of these parameters is related, through their effects on the shear layers that originate at the leading edges of the body, an attempt will be made to treat them separately.

4.1. *Flow normal to the prism*

The effect of turbulence on the pressure field. In their earlier study of these complex phenomena, Bearman & Trueman (1972) state the problem as follows. "It is known that two shear layers, free to interact, are basically unstable, and roll up to form discrete vortices. During formation, the growing vortices and, to a lesser extent, the shear layers draw in fluid from the base region; this continual entrainment process governs the value of the base pressure. The base pressure determines the amount of vorticity that is being shed from each side of the body and this in turn is related to the distance required for vortex formation and to the strength of the fully formed vortices. There are, therefore, some complex equilibria set up between the vorticity being shed from the body, the distance at which the vortices are formed, and the base pressure." Bearman (1967) and Bearman & Trueman (1972) showed that, the further from the body the vortices are formed, the higher is the base pressure.

From figures 1 and 3, it is evident that the dominant effect of introducing higher levels of turbulence intensity into the incident flow is to increase the pressure on the base (face (*c*)), and thus reduce the drag. Hence, we must now relate the way in which increasing the turbulence level alters the shear layer and vortex formation patterns to bring about these changes.

The mean pressure distribution around the prism, shown in figure 1, indicates that, in addition to increasing the base pressure, an increase in the level of turbulence intensity in the incident flow leads to more complete pressure recovery towards the rear of the sides of the prism (faces (*b*) and (*d*)). For uniform flow and for flow with a 4·4 % turbulence intensity (grid A1), there is no appreciable pressure recovery. This recovery occurs only for flows with turbulence levels above 6·5 % (grids A2, A3 and A4). The results of Pocha (1971) also indicate this pressure recovery, though no measurement of the turbulence level of his flow is given.

In figure 6 the r.m.s. fluctuating pressure distribution C'_p is shown for all flow conditions. On the front face of the body (face (*a*)), the increasing turbulence intensity results in an increase in the level of C'_p. However, on the base of the prism (face (*c*)), the increase in turbulence has the opposite effect (i.e. the general level of pressure fluctuations decreases).

These observations may be explained in the following manner. In the absence of turbulence in the incident flow, the shear layers originating at the front corners of the prism curve outward and form the familiar vortex street in the

wake close behind the body. The proximity of this vortex formation region gives rise to the high level of r.m.s. pressure fluctuations experienced on face (*c*) in addition to the low base pressure and high drag. When turbulence is added to the incident flow, both the increased entrainment of the surrounding fluid and the growth of inherent instabilities will cause the mean shear layers to thicken. This thickening may also be partly attributable to movement of the position of the shear layers. In addition to the thickening process, it is also possible that the centre-line of the mean shear layer will be bent further inward towards the sides of the body by a lower pressure caused by increased entrainment. The result of either or both of these processes is that there will be an intermittent reattachment of the mean shear layer to the side face (face (*b*) or (*d*)). This will inhibit vortex formation immediately behind the body, as occurs in uniform flow. Hence, the result of adding turbulence to the incident flow will be to cause weaker vortices to form further downstream, thus reducing C'_p on face (*c*).

The C'_p distribution on the side face of the prism (face (*b*) or (*d*)) is presented and compared with the smooth flow data of Vickery (1966), Chaplin & Shaw (1971) and Pocha (1971) in figure 6. The pattern emerges for a smooth incident flow of a C'_p distribution having dominant peaks at approximately $\frac{1}{4}D$ and $\frac{3}{4}D$ downstream from the front corner, caused possibly by movement of the points of separation and reattachment of a separation bubble on the side face beneath the shear layer. This conclusion is supported by the flow visualization experiments of Mulhearn (1973). The addition of small amounts of turbulence to the flow does not alter the overall pattern, but decreases the magnitude of the peaks in C'_p. The distribution of C'_p for 12·5 % turbulence intensity (grid A4) shows the rear peak to move forward to almost $\frac{1}{2}D$ under these conditions.

The axial correlation of the fluctuating pressures on the front face of the prism (face (*a*)) is presented in figure 7. The uniform flow data agree well with those of both Vickery (1966) and Pocha (1971) and give an associated axial correlation length scale of $4{\cdot}1D$ compared with Vickery's figure of $5{\cdot}6D$. The addition of turbulence to the flow has the effect of producing a decay in the correlation coefficient within a relatively short distance.

Figures 8 and 9 present the axial correlations of the fluctuating pressure on the side face of the body (face (*b*)) at approximately the mid-point ($\frac{5}{12}D$) and close to the rear corner ($\frac{11}{12}D$), respectively. It has been suggested that the addition of turbulence to the incident flow will cause the shear layers to intermittently reattach to the side wall of the prism. At the $\frac{5}{12}D$ correlation position the axial correlation for the 12·5 % turbulence flow (grid A4) is noticeably lower than the other correlations. Since the shear layers contain large, high-frequency instabilities, it is to be expected that the intermittent reattachment of the shear layers to the side walls (referred to previously for the 12·5 % turbulence flow case) will cause an axial distribution of C'_p which is poorly correlated despite the overall cyclic pattern of vortex shedding. At the $\frac{11}{12}D$ correlation position there appears a gradual effect where, for all the turbulent incident flows, an increasing reduction in the degree of correlation is measured as the turbulence level is increased. A comparison of the uniform flow axial correlation at each of the positions shows that it does not change over the length of the side

face, indicating that the associated shear layer does not interfere with the face at all.

The circumferential correlations of the surface pressure fluctuations are shown in figure 10, in which all the correlations are normalized with respect to a position approximately half way along the side face (face (*b*)). For all the flow conditions, there is a minimum in the correlation distribution at the rear of the side face, possibly due to the presence of the shear layer. The magnitude of the correlation coefficient at this point is reduced as the intensity of turbulence is increased. The degree of antisymmetric correlation between the two opposite sides of the model (faces (*b*) and (*d*)), caused by the alternate shedding of vortices, is reduced in the presence of an incident flow having a turbulence intensity of 12·5 % (grid A4), indicating a generally lower level of energy associated with the vortex-shedding process.

Eigenvector analysis. The representation of the surface pressure field of a bluff body as a random function of space and time in terms of a matrix of covariances is often inconvenient, for an adequate definition of the function usually requires a high-order matrix. It is difficult to get an understanding of these fluctuations from a large covariance matrix, since many different physical causes may contribute to them. It is often more convenient to represent such a random function as a series of modes. Such a series of modes can be obtained from the covariance matrix by eigenvector analysis using suitable algorithms (Boothroyd 1967; Wilkinson 1962; Barth, Martin & Wilkinson 1967). It can be shown that the sum of the eigenvalues is equal to the integral of the mean-square pressure fluctuations over the circumference of the body, and that each eigenvalue represents the energy contained in its associated spatial eigenvector distribution. It is suggested that it is possible to assign a physical significance to the dominant eigenvector distributions.

In table 3 the eigenvalues are normalized, such that their sum is proportional to the integral of the pressure energy around the circumference, and indicates the relative levels of total fluctuating energy acting on the body. The values obtained for each flow condition at $\alpha = 0°$ are

uniform flow	= 6·31,
grid A1 (4·4 % turbulence intensity)	= 4·21,
grid A2 (6·5 % turbulence intensity)	= 4·00,
grid A3 (8·0 % turbulence intensity)	= 3·81,
grid A4 (12·5 % turbulence intensity)	= 2·33.

It is seen that the total fluctuating pressure energy is reduced by the addition of turbulence to the incident flow. This reduction can be explained in physical terms by an examination of the dominant eigenvector distribution. This is plotted in figure 14 for $\alpha = 0°$. This distribution represents the vortex-shedding pressure mode by its strong antisymmetry about the mid points of the front and rear faces (faces (*a*) and (*c*)).

Thus, from table 3, the pressure energy associated with vortex shedding alone, for all five flow conditions at $\alpha = 0°$, is

$$\text{uniform flow} = 79{\cdot}7\,\% \text{ of } 6{\cdot}31 = 5{\cdot}03,$$

grid A1 (4·4 % turbulence) = 80·2 % of 4·21 = 3·38,
grid A2 (6·5 % turbulence) = 76·0 % of 4·00 = 3·04,
grid A3 (8·0 % turbulence) = 77·9 % of 3·81 = 2·97,
grid A4 (12·5 % turbulence) = 49·2 % of 2·33 = 1·15.

These figures show that the variation in the level of pressure energy associated with the vortex-shedding mode alone almost completely accounts for the variation in the total pressure energy levels for the different flow conditions. Figure 14 also shows that, although the energy levels associated with vortex shedding differ dramatically, the shape of the mode pattern (i.e. the eigenvector distribution) is almost identical for all the flow conditions.

Spectral analysis. Figures 15 and 16 illustrate the reduction of the effects of vortex shedding towards the rear of the side face (face (*b*)) by the introduction of increasing amounts of turbulence into the flow. Figure 15 shows the spectra at positions $\frac{7}{12}D$, $\frac{9}{12}D$ and $\frac{11}{12}D$ downstream of the leading edge corner on the side face of the prism at $\alpha = 0°$ in the 12·5 % turbulence flow case (grid A4). Although the C'_p at each of these positions is similar (C'_p = 0·384, 0·354 and 0·363, respectively), the magnitude of the vortex-shedding peak falls off sharply as the rear corner is approached, giving peak values of the spectral density of 5×10^{-2}, $3{\cdot}4 \times 10^{-2}$ and $2{\cdot}1 \times 10^{-2}$, respectively. This loss of energy at the vortex-shedding frequency is then primarily made up by an increase in the energy available at higher frequencies. Figure 16, showing the corresponding behaviour in a less turbulent incident flow (8·0 % turbulence), indicates a similar phenomenon.

A comparison of the magnitudes of the vortex-shedding peaks, at similar positions in the two different incident flows, reveals the general decrease of vortex-shedding activity, accompanied by an increase in incident flow turbulence. At $\frac{7}{12}D$ downstream of the front corner, the value of the spectral density at the vortex-shedding peak falls from $4{\cdot}6 \times 10^{-1}$ to 5×10^{-2} as the incident turbulence is increased from 8·0 to 12·5 %, even though C'_p changes only from 0·536 to 0·384. Corresponding reductions also occur at positions $\frac{9}{12}D$ and $\frac{11}{12}D$ downstream of the front corner. This behaviour pattern also holds for the other incident flow conditions.

4.2. *Flow at an angle to the prism*

Section 4.1 suggested that the effect of introducing turbulence into the incident flow is to alter the path taken by the shear layers from their point of origin at the front corners of the body to the vortex formation region. The dominant effect of rotating the prism with respect to the flow is also to alter the path of the shear layers. Thus, it is important to distinguish between the effects of body rotation and those of increased turbulence. In the following discussion, it will be assumed that the prism is rotated such that, at $\alpha = 45°$, the junction of faces (*a*) and (*b*) is pointing directly into the flow. Face (*a*) is still referred to as the front face, face (*b*) and face (*d*) as the side faces, and face (*c*) as the base.

The mean pressure distribution around the prism at α = 12·5 % is shown in

figure 2 for all the flow conditions. The pressure recovery at the rear of the side face (face (*b*)) is seen to increase with an increasing amount of turbulence in the incident flow following the trend established at $\alpha = 0°$ (see figure 1). As α is increased, the pressure rises on the base of the prism (face (*c*)), but the rise decreases as the turbulence level is increased, so that, for 12·5 % turbulence, the base pressure distribution remains constant at $C_p \simeq -0{\cdot}80$ for both values of α.

The mean drag coefficient C_D is shown in figure 3 for $0 \leqslant \alpha \leqslant 45°$. The overall behaviour of the drag is for it to decrease from a high initial value to a minimum in the region $8 < \alpha < 15°$, and subsequently to increase steadily until $\alpha = 45°$. It is postulated that the reason for this behaviour is that, at $\alpha = 0°$, the shear layer originating at the (*a*)/(*b*) corner swings outwards, and behaves in the manner described in §4.1. As the value of α is increased, this shear layer intermittently touches the rear corner, and subsequently adheres to the rear part of the side face (face (*b*)). When this value of α is reached, the shear layer, which at $\alpha = 0°$ left the prism at the (*a*)/(*b*) corner, now leaves it at the (*b*)/(*a*) corner, with the result that the shear layers are closer together. Thus, from Bearman & Trueman (1972), we may presume that the vortex formation region moves downstream, since the base pressure is observed to rise and the drag to fall. The effect of increasing the turbulence level of the incident flow is for the minimum in the drag curve to occur at smaller values of α. For 12·5 % turbulence intensity, the minimum occurs at $\alpha = 8°$; for 8 %, at 9° 30′; for 6·5 %, at 10°; for 4 %, at 12°; and for uniform flow, at 12° 30′. Further increases in α cause the drag to increase. The effect of turbulence in the incident flow is complex. For the prism normal to the flow, the effect of increased turbulence has already been explained in terms of a thickening of the shear layers, and their subsequent deflexion by the ends of the prism, creating a lower drag. This trend is seen to continue up to the angle at which steady reattachment to the side face (face (*b*)) occurs, the angle being smaller for more turbulent flows.

The variation in the mean lift developed on the prism with angle of incidence is shown in figure 4. Like the variation of mean drag with angle of incidence, this also shows a minimum value at the angle presumed to be associated with the steady reattachment of the shear layer to the side face (face (*b*)), this angle decreasing steadily with increasing turbulence. When the shear layer from the (*a*)/(*b*) corner has just reattached to the side wall, there is a strong totally enclosed separation bubble on face (*b*), which would cause higher local suctions than those on face (*d*); hence a negative lift is developed. Increasing the amount of turbulence in the flow may have two possible effects on the lift. First, the thickening of the shear layer may cause the total enclosure of the separation bubble to occur at a smaller angle; second, the thicker shear layer may result in a smaller separation area with less local suction; hence the value of the negative lift will decrease. Both these effects are shown in figure 8.

The variation of base pressure with flow angle is shown in figure 5. (Base pressure is defined as the average pressure at the mid and quarter points on face (*c*).) The magnitude of the base pressure is determined almost solely by the manner in which the shear layers leave the body and roll up to form discrete

vortices. Thus a low base pressure (a large negative value) is associated with vortex formation close to the body, while a high base pressure is caused by vortex formation further away. Hence, figure 5 leads to the conclusion that the steady reattachment of the shear layer to face (*b*) is associated with a deflexion of the shear layer and a distant region of vortex formation, while at lower and larger angles of incidence the vortices form close to the body.

The circumferential correlations of fluctuating pressures around the prism are shown in figure 11 for an angle of incidence $\alpha = 15°$. Here the pressures are correlated with respect to a point $\frac{1}{12}D$ downstream of the (*a*)/(*b*) corner. It was suggested earlier in the discussion on flow normal to the prism that the fall in the correlation coefficient on the side face (face (*b*)) is due to the intermittent impingement of a shear layer containing poorly-correlated high-frequency components. From figure 11 for flow at $\alpha = 15°$, we may postulate that the minimum in the distribution is directly related to the position of reattachment of the shear layer. A comparison of figures 10 and 11 then shows that the effect of rotation is to cause earlier reattachment. The effect of increasing the turbulence level is clearly seen in figure 11 to cause earlier reattachment of the shear layer by the manner in which the minimum in the correlation coefficient is brought forward along the side face (face (*b*)). In addition to the behaviour of the correlation coefficient on the side face (face (*b*)), it is evident that the effect of increasing the turbulence level is to cause an overall reduction in the correlation coefficient, this dilution effect being caused by a general increase in the high-frequency component of the pressure signal.

The fluctuating lift and drag experienced by the prism are resolved into components along the X and Y body axes and are shown in figures 12 and 13, respectively. The reason for the variation of C'_Y with α (figure 13) can be explained in terms of the way in which the correlation of the fluctuating pressures on opposite side faces is reduced by the reattachment of the shear layer. The variation of C'_Y with increase in the turbulence level at $\alpha = 0°$ is due to both a decrease in the C'_p level (shown in figure 6), and a decrease in the magnitude of the correlation between the side faces (shown in figure 10). As the prism is rotated, a similar variation of C'_Y is obtained, until reattachment has occurred, after which the value of C'_Y remains substantially constant.

4.3. *The Strouhal number*

The variation of the Strouhal number with the incidence of the flow and the amount of turbulence in the stream is shown in figure 17. The increase of the Strouhal number to a maximum at the angle at which the flow reattaches to the side face can be explained on the basis of the variation of the mean drag with angle of incidence. The minimum value of the mean drag in the region 12 to 15° is thought to be associated with a minimum wake width, and hence with a minimum longitudinal vortex spacing, if a constant ratio of vortex spacing to wake width is presumed. This would lead to an increase in the frequency of vortex shedding, and thus to an increase in the Strouhal number.

Both Roshko (1954) and Bearman (1967) proposed universal Strouhal numbers that correlate two-dimensional prism data. The universal Strouhal number

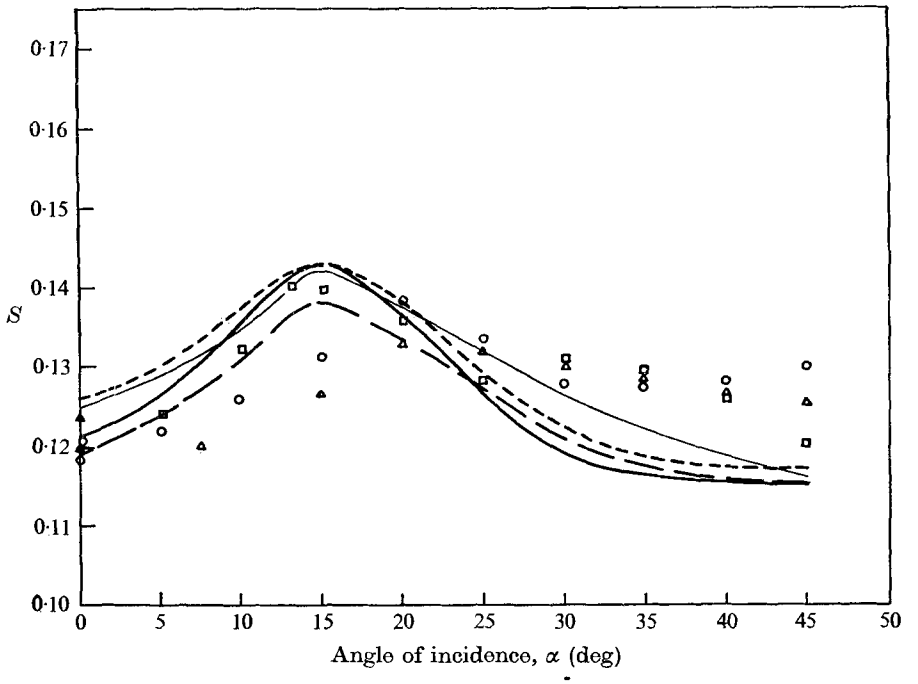

FIGURE 17. Variation of Strouhal number with flow direction. Vickery (1966): ○, smooth flow; △, turbulent. ▲, Bearman (1967), smooth flow. (For key to other symbols, see caption to figure 1.)

proposed by Roshko is based on a length scale equal to the wake width, derived by a notched hodograph technique, and a velocity scale equal to the velocity at the edge of the shear layer at the separation point, which is related to the base pressure. However, since both Gerrard (1966) and Batham (1973) have shown the Roshko universal Strouhal number to be influenced by the level of free-stream turbulence, its usefulness is considered doubtful, and has not been evaluated. The universal Strouhal number proposed by Bearman (1967) employed the same velocity scale as that of Roshko but a different length scale, the transverse distance between vortex rows. This was determined from the von Kármán vortex street drag coefficient, and used the Kronauer condition of minimum drag, rather than the von Kármán stability criterion. Bearman's universal Strouhal number may be written as

$$S_B = S\frac{l}{k}\frac{b}{h}.$$

S is the Strouhal number, k is $\{1-C_{pB}\}^{\frac{1}{2}}$ and b and h are vortex-street spacing parameters. For several bluff body shapes with and without base bleed, Bearman shows that $S_B = 0{\cdot}181$ over a wide range of variation of k. In the present experiments, the value of S_B was evaluated for each flow condition for angles of incidence of $\alpha = 0$, 15, 30 and 45°; and S_B was found to vary from 0·172 to 0·187. From the manner of the definition of S_B, it can be shown that the base pressure is related uniquely to the product of the Strouhal number and the drag coefficient,

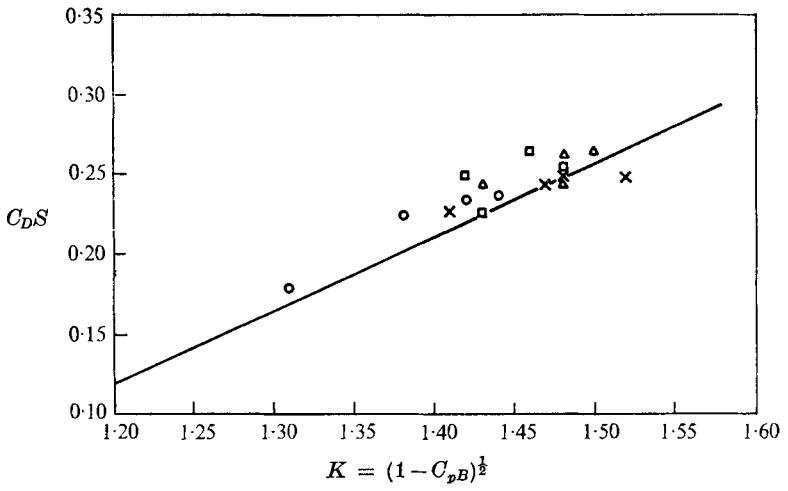

FIGURE 18. Bluff body wake similarity. α (deg): 0, 15, 30, 45. ———, Bearman (1967); ×, uniform flow.

Grid	A2	A3	A4
	▲	□	○

and, from this relationship, it is possible to determine the vortex-shedding frequency of a bluff body from its pressure distribution. The outcome of this in the present study is shown in figure 18, where good agreement with Bearman's data is obtained.

5. Conclusions

(i) The effect of increasing the intensity of turbulence in the flow normal to the prism is to produce a more complete pressure recovery on the side faces and a rise in the base pressure, leading to a reduction in the mean drag.

(ii) When the turbulence intensity is increased, it is inferred that the changes in the mean pressure distribution are influenced by changes in the behaviour of the shear layers. In addition to the spectral analysis of the fluctuating surface pressures, the axial and circumferential correlations suggest that increasing the turbulence intensity in the incident flow causes the shear layers to reattach intermittently to the rear of the side faces. The subsequent deflexions of the shear layers cause the vortex formation region to move downstream, thus raising the base pressure.

(iii) The eigenvector analysis is shown to be a useful method of analysing the fluctuating surface pressure field. The first eigenvector distribution, which depicts the vortex-shedding pressure mode, shows that the associated pressure energy is reduced by a factor of 5 when the turbulence intensity of the incident flow is increased from 0·5 to 12·5 %.

(iv) When the prism is rotated with respect to the flow, the base pressure rises and the drag falls. This is inferred, from the spectral analysis of the fluctuating pressures and the circumferential correlation distributions, to be caused by

the impingement of the shear layers on the side walls. Their subsequent deflexion causes the vortex formation region to move downstream. The addition of turbulence to the incident flow causes these phenomena to take place at smaller angles of incidence. Further rotation of the prism produces a fall in the base pressure as the vortex formation region moves upstream after the flow has re-attached to the side walls.

(v) The Strouhal number is shown to increase to a maximum at the angle at which the mean drag is a minimum.

(vi) The universal Strouhal number proposed by Bearman has been evaluated for all flow conditions with the prism at various angles to the flow and very good agreement with Bearman's proposed value is obtained for all cases, supporting his theory of bluff body wake similarity.

This work was performed while the author was employed at the Central Electricity Research Laboratories of CEGB. The advice of Mr J. Armitt is gratefully acknowledged.

REFERENCES

ALLEN, H. J. & VINCENTI, W. G. 1944 *N.A.C.A. Rep.* no. 782.

BARTH, W., MARTIN, R. S. & WILKINSON, J. H. 1967 *Num. Math.* **9**, 386.

BATHAM, J. P. 1973 *J. Fluid Mech.* **57**, 209.

BEARMAN, P. W. 1967 *J. Fluid Mech.* **28**, 625.

BEARMAN, P. W. & TRUEMAN, D. M. 1972 *Aero. Quart.* **23**, 229.

BOOTHROYD, J. 1967 *J. Am. Comp. Math.* **10** (3), algorithm 297.

CHAPLIN, J. R. & SHAW, T. L. 1971 *Proc. 14th Cong. IAHR*, Paris, vol. 2, p. 25.

GERRARD, J. H. 1966 *J. Fluid Mech.* **25**, 401.

MULHEARN, P. J. 1973 *Nature, Physical Science*, **241**, 165.

POCHA, J. J. 1971 Ph.D. thesis, Department of Aeronautical Engineering, Queen Mary College.

ROSHKO, A. 1954 *N.A.C.A. Tech. Note*, no. 3169.

VICKERY, B. J. 1966 *J. Fluid Mech.* **25**, 481.

WILKINSON, J. H. 1962 *Num. Math.* **4**, 354.